



Surface structure of yttrium-modified ceria catalysts and reaction pathways from ethanol to propene



Fumitaka Hayashi, Masashi Tanaka, Dongmei Lin, Masakazu Iwamoto*

Chemical Resources Laboratory, Tokyo Institute of Technology, 4259-R1-5 Nagatsuta, Midori-ku, Yokohama 226-8503, Japan

ARTICLE INFO

Article history:

Received 29 December 2013

Revised 9 April 2014

Accepted 27 April 2014

Keywords:

Ceria
Yttrium
Bioethanol
Propene
Heterogeneous catalysis

ABSTRACT

The additive effect of 31 metals on activity of ceria catalysts was studied for the conversion of ethanol to propene. Yttrium gave the best results and the propene yield showed a volcano-shaped dependence on the Y amount, being maximized at 20 atom% Y to that of Ce. The catalyst was stable due to very small carbon deposition rate which was approximately 1/100 of that on the parent CeO₂ catalyst. The water addition increased the propene yield to 30%, decreased the ethene yield to 37%, and did not change the durability. The physicochemical characterization of the Y/CeO₂ catalysts indicated that the surface of active catalysts was covered with a solid solution of CeO₂ and Y₂O₃. Pulse experiments of various candidate compounds suggested that the reaction pathways were ethanol → acetaldehyde → ethyl acetate → acetic acid → acetone → 2-propanol → propene through Tishchenko reaction, ketonization, and Meerwein–Ponndorf–Verley reduction.

© 2014 Elsevier Inc. All rights reserved.

1. Introduction

Propene is one of the most important ingredients in petroleum chemistry and its needs continuously increase because of growing production of propene derivatives, such as polypropene, propene oxide, and acetonitrile [1]. Today, propene is produced through hydrothermal cracking of naphtha. Depletion in fossil fuel and increased concerns on the environment stimulate replacing petroleum with renewable resources. Several researchers including us have suggested that bioethanol is a promising renewable platform chemical to yield various C₃ and C₄ compounds [2–13]. The present study was thus devoted to the conversion of ethanol to propene.

Zeolite catalysts are well known to show 20–30% of propene yield, except for short-term high yields, but this selectivity decreased with duration [14–17]. Oligomerization, cracking, and aromatization proceed on the acid sites of the zeolite pore, and propene is selectively produced as a result of shape selectivity of the pore window. Such uncontrolled reactions, however, result in coke formation and short lifetimes of catalysts. On the other hand, Ni-ion-loaded MCM-41 [8] and Sc-modified In₂O₃ catalysts [9,10] offered new types of catalysis for the production of propene without shape selectivity, but the catalytic activity gradually decreased with duration at 30 vol% of ethanol (the high

concentration of ethanol is essential to reduce running costs of the industrial processes). Therefore, new catalysts workable under the practical conditions are needed to produce propene from bioethanol.

Various metal oxide-based catalysts have been examined as catalysts for the conversion of ethanol, but most of the products besides ethene are oxygenated compounds, such as aldehydes, ketones, and higher alcohols [2–7,18–21]. Our attention was paid to the selective conversion of C_x-alcohol to C_{2x-1}-ketone on ceria-based catalysts [2–6] and assumed that any acetone formed could be hydrogenated and subsequently dehydrated by controlling the acid-base and redox properties of catalysts. Indeed, yttrium-loaded CeO₂ was found by us to show the stable catalytic activity for the selective conversion of ethanol to propene [12]. In this study, we first examined the additive effect of 31 metals on the ceria catalysts in the absence and presence of water. Niobium and yttrium were then selected as effective additives and the dependences of activity on their added amounts were studied. Second, effect of the preparation method was examined for the better catalyst, Y/CeO₂. The structural, redox, and acid-base properties of Y/CeO₂ were characterized to reveal the correlation between the catalytic activity and the properties. Last, the reaction pathways were discussed on the basis of the results of product distributions in the continuous flow and pulse reactions.

* Corresponding author. Fax: +81 3 3817 1612.

E-mail address: iwamotom@tamacc.chuo-u.ac.jp (M. Iwamoto).

2. Experimental

2.1. Preparation of metal-modified ceria catalysts

Ceria-based catalysts were prepared using a conventional impregnation method or a co-precipitation method. In the former, the parent ceria, obtained from Catalysis Society of Japan (JRC-CEO-3, 85 m² g⁻¹), was impregnated using aqueous solutions of the metal salts: nitrates of Li, Mg, Ca, Y, La, Sm, Er, Mn, Fe, Co, Ni, Cu, Zn, Rh, Cd, Al, In, and Bi, acetates of Sc and Sn, ammonium salts of Ti, V, Nb, Mo, W, and Re, alkoxides of Ta and Si, and chloride of Ir. In the latter, Ce(NO₃)₃·6H₂O, Y(NO₃)₃·6H₂O, and ammonium hydrogen carbonate were used as precursors and a precipitant, respectively, and the solid solution was prepared according to the literature [22]. All samples were calcined at 873 K for 5 h in air. Catalysts prepared by the impregnation and the co-precipitation method are denoted by M(x)/CeO₂ and M(x)-CeO₂, respectively, where M and x represent the metal used and the atomic % to that of Ce.

2.2. Measurement of catalytic activity

Ethanol (>99.5%, Kanto chemical) was used without further purification. The continuous flow reactions were conducted in a fixed-bed plug-flow reactor made of quartz (i.d. 10 mm) at an atmospheric pressure under the following conditions: catalyst weight 0.05–2.0 g (particle diameter, 300–600 μm), total flow rate 12–32 ml min⁻¹, partial pressure of ethanol (P_{EtOH}) 30 vol%, P_{H₂O} 0–30 vol%, N₂ balance. Before the catalytic runs, the catalysts were heated in a N₂ flow at 673 K for 1 h. The products were analyzed with an online automatic gas chromatograph (AG-1, Round Science) equipped with four kinds of packed columns: (1) activated charcoal, (2) MS 5A, (3) Porapak Q, and (4) PEG-20 M. The columns 1–3 were independently connected to the three TCD detectors to determine the yields of ethene, CO, and CO₂. The column 4 was connected to the FID detector to determine the yields of other carbon products. The C₄–C₇ hydrocarbons and oxygenated products were analyzed as needed with an offline FID gas chromatograph (GC-2014, Shimadzu) with a capillary column of CP-7561 (10 m, Varian) or GS-Q (30 m, Agilent). Conversion levels of ethanol and yields of carbon products (C_nH_xO_y, n = carbon number) were calculated by Eqs. (1) and (2), where the partial pressures of ethanol before and after the reaction are denoted by P_{EtOH} and P'_{EtOH}, respectively.

$$\text{Ethanol conv. (\%)} = 100(1 - (P'_{\text{EtOH}}/P_{\text{EtOH}})(P_{\text{N}_2}/P'_{\text{N}_2})) \quad (1)$$

$$C_n \text{ Yield (\%)} = 100(n P'_{\text{C}_n}/2P_{\text{EtOH}})(P_{\text{N}_2}/P'_{\text{N}_2}) \quad (2)$$

For pulse experiments, ethyl acetate (>99.5%, Kanto chemical), acetic acid (>99.5%, Kanto chemical), acetone (>99.9%, Aldrich), and ethanol (>99.5%, Kanto chemical) were used as substrates without further purification. Each substrate with volume of 2 μl was fed into the catalyst bed in the quartz glass reactor (i.d. 7.6 mm) at 403 K under the following conditions: catalyst weight 0.1 g (particle diameter, 300–600 μm), total flow rate 10–80 ml min⁻¹, N₂ balance. As needed, ethanol, water, or H₂ gas was used as a co-reactant. The pretreatment and the product analysis methods were the same as those for the continuous flow reactions.

2.3. Characterization

N₂ adsorption isotherms were determined at 77 K with an automatic gas sorption meter BEL Japan Belsorp mini II. Before the measurements, the samples were degassed at 423 K for 2 h in

vacuum. Field-emission scanning electron microscopy, FE-SEM, images were collected with a Hitachi HR-S5500. Powder X-ray diffraction, PXRD, patterns were measured using a Rigaku Ultima IV diffractometer with monochromated Cu Kα radiation (λ = 0.15418 nm, 40 kV, 40 mA). Temperature-programmed reduction with hydrogen, H₂-TPR, profiles were recorded with a BEL Japan BelCat. X-ray photoelectron (XP) spectra were measured with an Omicron EA125 XPS system. All binding energies were corrected using the values of C 1s (285.0 eV). X-ray absorption fine structure, XAFS, analysis was carried out at the BL-9C station of the Photon Factory at the High Energy Accelerator Research Organization, Japan. The energy and current of electrons in the storage ring were 2.5 GeV and 350 mA, respectively. Energy calibration was performed using a Cu foil (8.9788 keV). Prior to the measurements, the samples were evacuated at 673 K. Data analysis was performed using the REX2000 program (Ver. 2.5.9, Rigaku). The k³-weighted extended X-ray absorption fine structure, EXAFS, oscillation was Fourier-transformed (FT) into the r space using the k range of 3.0–14.0 Å⁻¹ for Y or 3.0–10.0 Å⁻¹ for Ce. Curve fitting analysis was carried out in the r range 1.2–2.2 Å for the Y–O contribution or 1.5–2.3 Å for the Ce–O to calculate the average nearest neighbor coordination number and the average bond lengths of Y–O and Ce–O. Backscattering amplitudes and phase-shift functions were calculated from the crystal structures of Y₂O₃ and CeO₂ using the FEFF6 code.

Diffuse reflectance infrared Fourier transform (DRIFT) spectra were measured in a DR-600Bi diffuse reflectance cell using Jasco FTIR-6300 spectrometer equipped with a MCT detector. Self-supported KBr plates were used as windows for the cells. Scan times and a resolution were 32 and 4 cm⁻¹, respectively. The KBr powder evacuated at 303 K was used as a reference. Prior to the measurements, the sample was evacuated at 673 K for 1 h. Pyridine (>99.5%, Wako) or CO₂ (>99%, GL Sciences) was introduced onto the sample at 303 K for 5 min and then evacuated at the same temperature for 30 min. All spectra were recorded as the difference spectra before and after the introduction of adsorbates.

3. Results and discussion

3.1. Additive effect of metals on activity of ceria catalysts

Table 1 summarizes the activity of various ceria catalysts modified with mainly 10 atom% metal additives, in which the data after 0.75 h are shown because the activity was often changed with duration. The metals were listed in the sequence of the family. The surface areas of M(10)/CeO₂ are also summarized in the table and were roughly constant at 52–61 m² g⁻¹ independent of the metal additives.

The conversion degrees of ethanol were all 80–100% under the present reaction conditions. Among 31 metals, the addition of Y, Sm, Ti, Nb, or Ta increased the propene yield, while that of Fe, Co, Cu, Zn, Sn, or Bi increased the acetone yield. The formation of acetone on the latter group was well consistent with the previous reports on ZnO- and CeO₂-based catalysts [2–6] that were active for the conversions of C_x-alcohols to C_{2x-1} ketones. As shown in Run 18 of Table 1, the Nb(10)/CeO₂ catalyst exhibited the highest propene yield of 32%, but its activity was not stable. The deactivation with duration was also observed on the Ti- or Ta-modified CeO₂ catalyst. In contrast, the Y(10)/CeO₂ catalyst showed no deactivation during continuous service of 80 h, although the propene yield, 19% (Run 6), was lower than those on the Nb(10)/CeO₂ and the Ti(10)/CeO₂. Based on the high propene yield or the long life, the Nb- and Y-modified ceria were selected as the catalysts in the subsequent detailed study.

Table 1
Activity of various metal-modified ceria catalysts for the conversion of ethanol.^a

Run	Additive (atom%) ^b	S _{BET} (m ² g ⁻¹)	React. cond.		Conv. (%)	Yield of products on carbon basis (%)							A _{C₃/CO_x} ^c
			Temp.(K)	P _{H₂O} (vol%)		EtOH	C ₃ H ₆	Acetone	C ₂ H ₄	C ₄ H ₈	CO	CO ₂	
1	None	85	693	0	100	12	10	31	2	4	9	78	1.7
2	Li(10)	n.m. ^d	723	0	85	1	14	8	1	5	5	38	1.6
3	Mg(10)	n.m. ^d	723	0	100	13	5	29	6	6	13	83	0.9
4	Ca(10)	57	723	0	100	9	7	17	1	4	9	56	1.3
5	Sc(10)	n.m. ^d	723	0	100	9	3	24	0	3	8	55	1.1
6	Y(10)	59	723	0	100	19	0	37	1	3	12	79	1.2
7	Y(20)	54	703	0	100	25	0	52	1	2	8	92	2.5
8	Y(20)	54	703	30	100	30	2	37	0	3	9	86	2.7
9	Y(50)	45	723	0	>99	15	0	45	1	2	5	71	2.2
10	Y(25) _{Solid-Sol}	46	698	0	84	11	12	25	0	3	6	65	1.8
11	Y(67) _{Solid-Sol}	60	698	0	100	20	6	36	0	3	7	76	2.5
12	Y(150) _{Solid-Sol}	48	698	0	100	20	6	36	1	3	7	75	2.7
13	La(10)	n.m. ^d	723	0	100	11	4	33	0	4	9	70	1.2
14	Sm(10)	n.m. ^d	425	0	100	16	6	42	0	3	8	81	2.1
15	Er(10)	n.m. ^d	698	0	>99	10	3	21	3	3	11	58	0.9
16	Ti(10)	61	673	0	100	27	0	15	12	2	13	77	1.9
17	V(10)	n.m. ^d	723	0	100	9	0	8	8	1	9	72	0.9
18	Nb(10)	54	673	0	99	32	1	17	10	1	10	82	3.0
19	Nb(10)	54	698	30	100	32	12	7	4	3	17	81	2.2
20	Nb(20)	52	673	0	99	7	0	32	7	1	5	60	1.4
21	Ta(10)	n.m. ^d	698	0	100	26	2	15	8	2	12	71	2.1
22	Cr(10)	n.m. ^d	723	0	100	4	9	11	5	5	11	51	0.8
23	Mo(10)	n.m. ^d	723	0	98	7	3	28	19	1	4	80	1.9
24	W(10)	n.m. ^d	723	0	100	9	11	8	10	1	9	79	2.0
25	Mn(10)	n.m. ^d	723	0	100	5	6	13	0	6	12	49	0.6
26	Fe(20)	n.m. ^d	673	0	100	3	36	7	2	5	13	79	2.2
27	Co(10)	n.m. ^d	673	0	100	2	27	4	0	4	14	52	1.7
28	Ni(10)	n.m. ^d	673	0	99	2	9	0	1	6	13	57	0.6
29	Cu(10)	n.m. ^d	673	0	96	1	15	3	1	1	13	37	1.2
30	Zn(10)	n.m. ^d	673	0	98	2	16	3	4	2	13	40	1.2
31	Re(1)	n.m. ^d	723	0	100	5	11	2	6	8	12	49	0.8
32	Rh(1)	n.m. ^d	673	0	100	2	9	0	1	12	15	70	0.4
33	Ir(1)	n.m. ^d	723	0	>99	3	13	3	3	4	12	48	1.1
34	Cd(10)	n.m. ^d	698	0	>99	6	12	15	3	3	10	54	1.3
35	Al(10)	n.m. ^d	673	0	92	5	5	8	1	1	7	33	1.1
36	In(10)	n.m. ^d	723	0	100	5	11	13	7	7	14	62	0.8
37	Si(10)	n.m. ^d	723	0	99	15	4	15	4	5	12	62	1.1
38	Sn(10)	n.m. ^d	673	0	>99	1	23	3	2	2	13	46	1.6
39	Bi(10)	52	673	0	82	2	15	5	1	2	14	41	1.1
40	Y ₂ O ₃ ^e	10	723	0	79	7	4	46	0	1	2	61	4.6

^a Catalyst weight, 2.0 g; total flow rate, 12.8 ml/min; P_{EtOH}, 30 vol% (N₂ balance); total pressure, 0.1 MPa. All of the results were obtained after 45 min.

^b Additives were loaded using the impregnation or co-precipitation method. Subscript Solid-Sol represents the latter method, while no subscript symbol does the former.

^c Ratio of total yield of propene and acetone to that of CO₂ and CO.

^d Not measured.

^e C-type Y₂O₃ used as a catalyst for comparison.

The results on Nb addition will be introduced first. The effect of the amount of Nb on the catalytic activity is shown in Fig. 1a and in Table 1, Runs 18 and 20. The surface areas of the catalysts were decreased through the Nb addition from 85 to 52–54 m² g⁻¹ irrespective of the Nb amount. The propene yield was maximized at 10 atom% Nb, and it reached 32% as shown in Fig. 1a. The other byproducts were ethene, acetone, and butenes. Fig. 2a shows the stability of the Nb(10)/CeO₂ catalyst in the absence of water. The propene yield decreased with duration, and the acetone yield increased. The effect of water addition was further examined to prevent the deactivation. Fig. 2b shows the long-term experiment at P_{H₂O} = 30 vol%, and Fig. S1a (Supplementary material) shows the product distribution as a function of P_{H₂O}. The yield of propene became constant in the presence of water within the present experiment, but the yields of ethene and acetone changed gradually with the reaction time. As will be shown later, since acetone was an intermediate for the propene formation, the increase in the acetone yield indicated partial deactivation of the Nb(10)/CeO₂ catalyst. The detailed study on the Nb-modified catalyst was not continued here except for the measurement of carbon deposition.

Fig. 1b shows the effect of the amount of Y. The dependency was again of volcano shape, namely the yield of propene was maximized at 20 atom% Y. Fig. 2c and d show the long-term stability of the Y(20)/CeO₂ catalyst in the absence and presence of water, while Fig. S1b shows the product distribution as a function of P_{H₂O}. The yields of propene were constant at 25% and 30% during continuous experiments for 50–80 h, and the ethene yields were also constant at 50% and 37%, respectively. The findings indicated the high durability of Y/CeO₂ and the effectiveness of the water addition for the increase in the propene formation and decrease in the ethene formation. It is widely accepted that the dehydration of ethanol is well catalyzed on acid sites. The acidity on the Y/CeO₂ catalyst might be weakened by the addition of water [16]. The tolerance against water vapor is an advantage of the Y/CeO₂ catalyst over the zeolite catalysts, since the dealumination and the subsequent deactivation of zeolites are the significant problems.

The long-term stabilities of the catalysts were discussed from the viewpoint of carbon deposition. The thermogravimetric analyses gave the following carbon deposition rates (see Fig. 3): in the absence of water, 1.8, 2.6, 0.02, and 1.7–4.7 mg_{carbon} g_{cat}⁻¹ h⁻¹ on the pure CeO₂, Nb(10)/CeO₂, Y(20)/CeO₂, and H-ZSM-5 zeolites

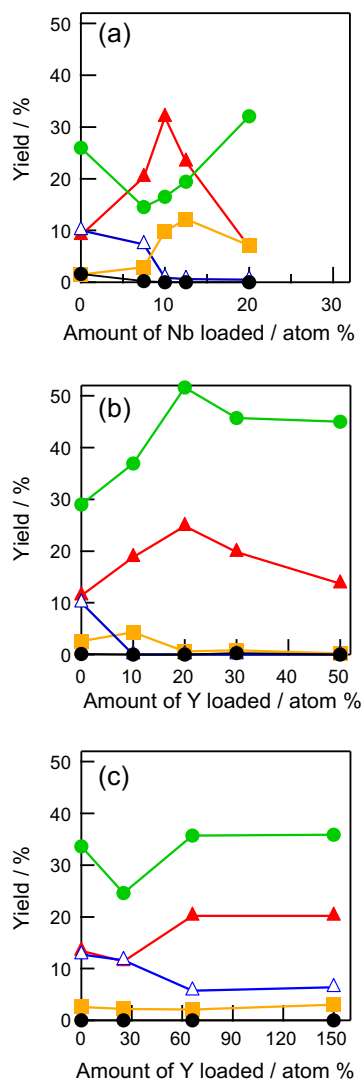


Fig. 1. Catalytic activity of Nb/CeO₂ (a), Y/CeO₂ (b), and Y-CeO₂ (c) as a function of the amount of Nb or Y loaded for the production of propene (red triangle), ethene (green circle), butenes (orange square), acetone (blue triangle), and acetaldehyde (black circle). The results obtained after 45 min are plotted. Reaction conditions: catalyst weight, 2.0 g; total flow rate, 12.8 ml min⁻¹; P_{EtOH}, 30 vol%; and reaction temperature, 693–723 K. (For interpretation of the references to color in this figure legend, the reader is referred to the web version of this article.)

[14,23] and in the presence of water (P_{H₂O} = 30 vol%) 0.6, 0.4, 0.06, and 0.6–1.6 mg_{carbon} g_{cat}⁻¹ h⁻¹, respectively. In the absence of water, the carbon deposition rate on the Y(20)/CeO₂ catalyst was approximately 1/100 of those on the Nb(10)/CeO₂ and zeolites. In the presence of water, most of the values were reduced, but that on the Y(20)/CeO₂ was still smaller than those on the Nb(10)/CeO₂ and zeolites. It was indicated that the Y(20)/CeO₂ would be the best catalyst for the stable conversion of ethanol to propene among the ceria-based catalysts.

3.2. Correlation of catalytic activity with physicochemical properties of Y/CeO₂

The co-precipitation of Y₂O₃ and CeO₂ (=Y-CeO₂) gave their solid solutions, which were employed here as reference catalysts. Their typical physicochemical properties and catalytic activity were briefly introduced. The surface areas of the Y-CeO₂ were 46–60 m² g⁻¹ (Runs 10–12, Table 1), being almost the same as those of the Y/CeO₂ (Runs 6–9). The activity is summarized in

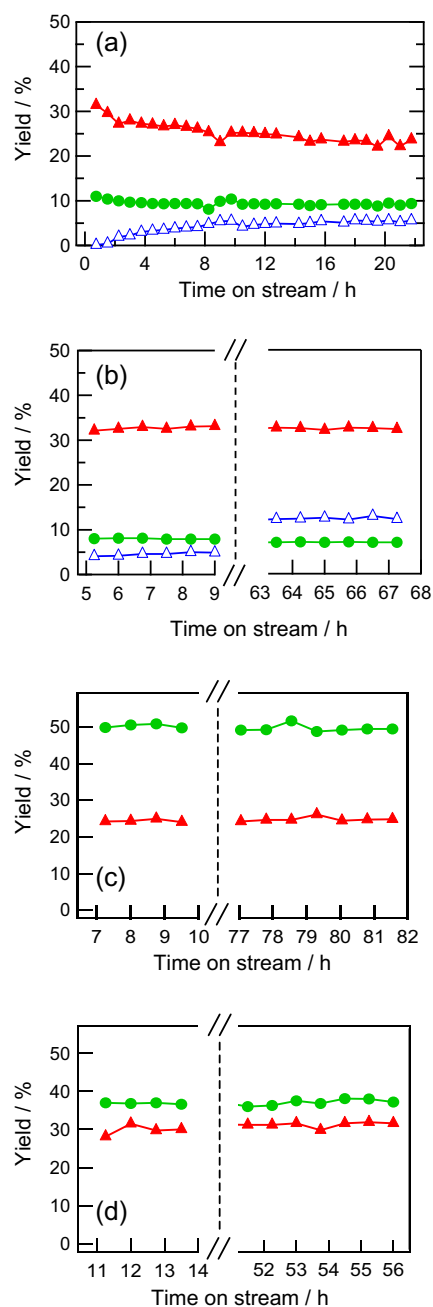


Fig. 2. Long-term experiments for the catalytic activity of Nb(10)/CeO₂ (a,b) and Y(20)/CeO₂ (c,d) in the absence and the presence of water. Symbols are the same as those in Fig. 1. Reaction conditions: catalyst weight, 2.0 g; total flow rate, 12.8 ml min⁻¹; P_{EtOH}, 30 vol%; P_{H₂O}, 0 (a,c) and 30 vol% (b,d); reaction temperature, 698 (a,b), 693 (c), and 703 K (d).

Fig. 1c. The propene yields on the Y(67)- and Y(150)-CeO₂ were both 21%, which was similar to 25% on the Y(20)/CeO₂. It would be worthy to note that the propene yield on pure Y₂O₃ was only 7% (Run 40, Table 1).

Fig. S2 shows the FE-SEM images of the CeO₂, Y(20)/CeO₂, and Y(67)-CeO₂. The parent CeO₂ was aggregates of nanoparticles with 10–20 nm diameters (Figs. S2a and S2b). The morphology of the Y(20)/CeO₂ was almost the same as that of CeO₂ (Figs. S2c vs. S2b), indicating no change with loading treatment of Y. The Y(67)-CeO₂ catalyst also showed the similar particle size and morphology to those of Y(20)/CeO₂ (Fig. S2d). Fig. S3 shows the PXRD patterns of the CeO₂, Y(20)/CeO₂, and Y(67)-CeO₂. All

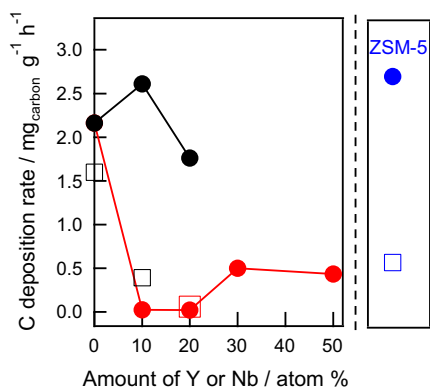


Fig. 3. Carbon deposition rate on Nb/CeO₂ (black symbols) and Y/CeO₂ (red symbols) as a function of the amount of Nb or Y loaded, together with that on the zeolites (blue symbols in the right panel) reported in Refs. [14,23]. Partial pressure of water: closed black, red, and blue circles, 0 vol%; open black and red squares, 30 vol%; blue square, 88 vol%. (For interpretation of the references to color in this figure legend, the reader is referred to the web version of this article.)

samples exhibited single-phase diffraction patterns assignable to the cubic fluorite structure of ceria (JCPDS No. 34-394, $a = 0.5410$ nm). The peak positions were little shifted upon the Y loading, indicating the high dispersion of Y ions in the ceria lattice. The FE-SEM and PXRD analyses indicated no noticeable difference between the Y/ and Y-CeO₂ samples.

It was reported that incorporation of Y³⁺ cations to tetravalent host ceria readily proceeded as a result of the similar ionic radius: The ionic radii of Ce⁴⁺ and Y³⁺ ions are 0.97 Å for the 8 coordination and 1.02 Å for the 6 coordination, respectively [24]. Such replacement by Y cations led to the formation of both oxygen vacancies and reduced Ce³⁺ ions [25]. The local structures of Y and Ce were

here studied by the XAFS analysis. Fig. 4a shows the Y-K-edge XANES spectra of the Y/ and Y-CeO₂. Two noticeable features were observed. First, all samples show no pre-edge peaks around 17030 eV, assignable to the 1s → 4d transition of Y. This s → d transition is partially allowed for the distortion of octahedral environment, only when p-orbitals are mixed with d orbitals. No appearance of this transition indicated little distortion of the octahedral symmetry, as has been reported in the other Y-containing systems [26]. The second point was change in the white line shape with the sample. All samples exhibited two peaks at 17050 and 17058 eV attributable to two inequivalent Y sites in the C-type bixbyite structure [27], although the peak shapes were different. The Y(10)/, Y(20)/, and Y(67)-CeO₂ samples gave almost the same spectra, indicating the equivalent distributions of Y in the fluorite structure. On the other hand, the C-type sesquioxide Y₂O₃ and heavily Y-doped Y(50)/CeO₂ exhibited the distinct increments in the 17058 eV. The change suggested the increase in the Y₂O₃ phase on these samples, which will be discussed in the following paragraphs in more detail.

The FT-EXAFS spectra shown in Fig. 4b gave valuable information on the local structure. The Y(50)/CeO₂ and C-type Y₂O₃ samples showed three bands: The first peak at 1.8 Å was due to the Y–O shell, and the second and third peaks at 3.1 and 3.8 Å were due to two Y–Y shells distributed at different distance [26,27]. In contrast, the Y(10)/, Y(20)/, and Y(67)-CeO₂ samples showed two significant signals at 1.8 and 3.6 Å, which were attributed to the Y–O and Y–O–Ce shells, respectively. The Y(20)/CeO₂ sample also gave a small peak at 3.1 Å due to the Y–O–Y shell. The appearance of the 3.6 Å peaks for the Y(10)/, Y(20)/, and Y(67)-CeO₂ was interpreted as the evidence for the formation of solid solution of CeO₂ and Y₂O₃, and the disappearance of this peak for the Y(50)/CeO₂ was attributed to the formation of thick Y₂O₃ layers on the surface. The results of curve fitting analysis for Y species are summarized in Table S2. The coordination number, CN, for the solid solution

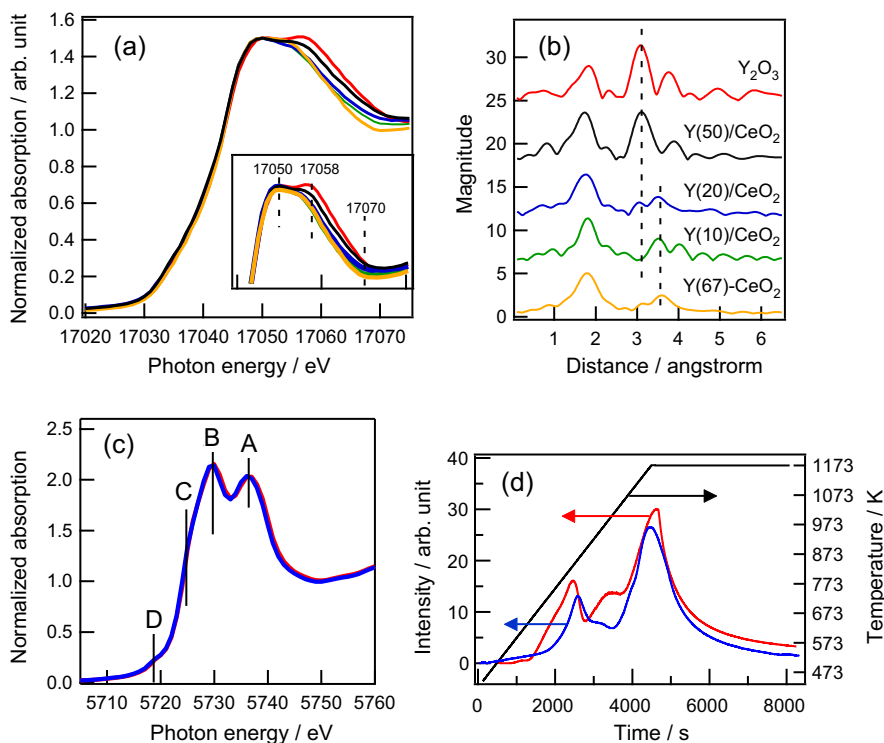


Fig. 4. Y-K-edge XANES (a) and EXAFS spectra (b) of Y(10)/CeO₂ (green), Y(20)/CeO₂ (blue), Y(50)/CeO₂ (black), Y(67)-CeO₂ (orange), and reference Y₂O₃ (red). Ce-L_{III}-edge XANES spectra (c) and H₂-TPR profiles (d) of Y(20)/CeO₂ (blue) and pure CeO₂ (red). Symbols A–D in (c) are the same as those in Refs. [30,31]. (For interpretation of the references to color in this figure legend, the reader is referred to the web version of this article.)

Y(67)–CeO₂ was 6.0, which agreed well with the results previously-reported [25,26]. Meanwhile, the CNs for the Y(10)/CeO₂, Y(20)/CeO₂, and Y(50)/CeO₂ were partly smaller (5.6–5.7), indicating the formation of coordinatively unsaturated Y species. The average Y–O bond lengths for the respective samples were ca. 2.25 Å, independent of the catalyst preparation method and amount of Y loading. The results could suggest the formation of the solid solution at low loading of Y and the increase in the Y₂O₃ phase at the high loading, although their amounts depended on the catalyst preparation methods.

Fig. 4c shows Ce-L_{III}-edge XANES spectra of the Y(20)/CeO₂ and pure CeO₂ samples. Pure CeO₂ was reported to usually possess oxygen vacancies of $1 \times 10^{12} - 1 \times 10^{14} \text{ cm}^{-2}$, whose amounts were dependent on the crystallite size [28,29]. The spectra showed four different lines named A, B, C, and D according to the literature [30,31]. The observed four lines were all characteristic of a Ce⁴⁺ ion, originating from the hybridization of Ce 4f and O 2p states in the initial state. It should be noted, however, that certain amounts of Ce³⁺ species might exist, because the peak position of Ce³⁺ was very close to that of the line C of Ce⁴⁺ ion (the difference was only 1.9 eV) [30,31]. The curve fitting analysis was thus conducted to roughly quantify the contents of Ce³⁺ ions and the results are summarized in Table S3. The average CN for CeO₂ and Y(20)/CeO₂ was 7.8 and 7.4, which were lower than 8.0 for oxygen vacancy-free ceria. When all decrement in the CN value was attributable to the formation of oxygen vacancies accompanied by the change of Ce⁴⁺ to Ce³⁺, approximately 30% of Ce was estimated to be reduced to Ce³⁺ in the Y(20)/CeO₂ [32].

Fig. 4d shows the TPR profiles of pure CeO₂ and Y(20)/CeO₂ to determine amounts of the oxygen vacancies. The pure CeO₂ exhibited three reduction peaks at 790, 950, and 1170 K. The first and second peaks were due to the reduction of surface oxygen ions, and the third one was due to the reduction of oxygen ions in the bulk [33–35]. The total amount of H₂ consumption on the CeO₂ was 2.63 mmol_{H₂} g⁻¹ based on the integrated peak areas, which was 90% of the amount (2.90 mmol_{H₂} g⁻¹) required to reduce defect-free ceria, CeO₂ + 1/2H₂ → CeO_{1.5} + 1/2H₂O. The observed difference of 10% could be attributed to oxygen vacancies around the Ce³⁺ ions, as has been suggested in the literature [28,29] and is shown in Table S3. The Y(20)/CeO₂ gave smaller first and second peaks and roughly the same third peak. The total amount of H₂ consumption observed was 2.26 mmol_{H₂} g⁻¹. The H₂ consumption for Ce_{0.833}Y_{0.167}O_{1.917}, which corresponds to the Y(20)/CeO₂ nominally composed of 83.3% CeO₂ and 16.7% YO_{1.5}, was estimated to be 2.57 mmol_{H₂} g_{cat}⁻¹ from the following equation: Ce_{0.833}Y_{0.167}O_{1.917} + 0.417H₂ → Ce_{0.833}Y_{0.167}O_{1.5} + 0.417H₂O. The assumption of 10% oxygen vacancies on the sample resulted in decrease in the H₂ amount to 2.31 mmol_{H₂} g_{cat}⁻¹. This value was in excellent agreement with the experimental value, 2.26. Fig. S4 shows the Ce 3d_{5/2} and 3d_{3/2} core level XP spectra of the CeO₂ and Y(20)/CeO₂ catalysts, and the assignment of each signal was summarized in Table S4. Here, the Ce³⁺ concentrations in the two samples were estimated according to the method in the literature [36,37], and the results for the peak deconvolution are shown in the figure. The Ce³⁺ concentrations (Ce³⁺/(Ce³⁺ + Ce⁴⁺)) of the CeO₂ and Y(20)/CeO₂ samples were estimated to be 16.9% and 19.1%, respectively, being well consistent with the results for the TPR analysis. It follows that the solid solution of CeO₂ and Y₂O₃ was generated through the Y loading and there was the almost same ratio of oxygen vacancies when the Y amount was not great.

Acid-base properties of the catalysts were investigated by the DRIFT analysis using pyridine and CO₂ as probe molecules. Fig. 5a shows the pyridine-adsorbed spectra. The CeO₂ exhibited absorption peaks at 1440, 1485, 1535, 1560, 1578, and 1600 cm⁻¹, in which the 1440 cm⁻¹ band was attributable to pyridine adsorbed on Lewis acid sites, the 1535 cm⁻¹ band on

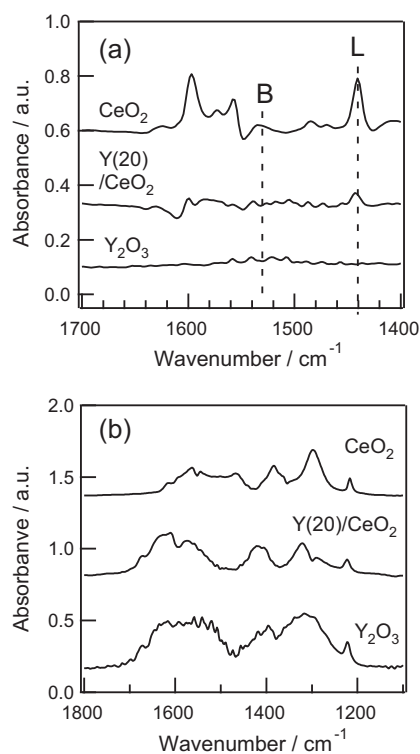


Fig. 5. Difference DRIFT spectra of pyridine (a) and CO₂ (b) adsorbed CeO₂, Y(20)/CeO₂, and Y₂O₃ after evacuation at 303 K. Capital letters L and B in (a) stand for the Lewis and Brønsted acid sites.

Brønsted acid sites, and the others on the Lewis acid sites or hydroxyl groups [38]. In contrast, the Y(20)/CeO₂ and Y₂O₃ gave very small peaks, indicating very few acid sites on their surfaces. This result indicated that the added Y₂O₃ diminished the strong acid sites on the ceria surface. Fig. 5b shows the CO₂-adsorbed DRIFT spectra. The assignment of CO₂ species is summarized in Fig. S4 [39–41]. In the five bands observed on the CeO₂, the bands at 1220, 1390, 1475, and 1590 cm⁻¹ were assigned to hydrogen carbonate, while those at 1300 and 1590 cm⁻¹ to bidentate carbonate. On the Y(20)/CeO₂, except for the 1220 cm⁻¹ band, all bands were blueshifted by ca. 25 cm⁻¹, and the spectrum turned out to be similar to that on Y₂O₃, indicating the formation of new basic sites. Both the pyridine and CO₂ adsorption experiments indicated that the addition of 20 atom% Y resulted in the formation of yttrium oxide-predominating surface.

Finally, the structures of Y-loaded ceria prepared by the impregnation method are shown schematically in Fig. 6 as a function of Y loading. Below 10 atom% Y, Y atoms were used for the formation of surface solid solution of CeO₂–Y₂O₃. At around 20 atom% Y, the surface and the inside of Y/CeO₂ were nearly covered with the solid solution. Too much Y loading (around 50 atom% Y) would cause the formation of thick Y₂O₃ layers. The requisite amount of Y₂O₃ for monolayer coverage of ceria was estimated to be 10.9 wt%_{catalyst} [42] according to the method in the literature [43]. The Y₂O₃ content in the Y(20)/CeO₂ was 11.6 wt%, supporting the formation of 1–2 layers of a surface solid solution.

3.3. Reaction pathways on Y-loaded CeO₂

The reaction pathways were investigated based on the product distributions in the continuous flow reactions and the pulse experiments. The total yields of carbon products summarized in Table 1 were 35–90% in all experiments, greatly depending on the kinds of metal additives. The discrepancy between the ethanol conversion

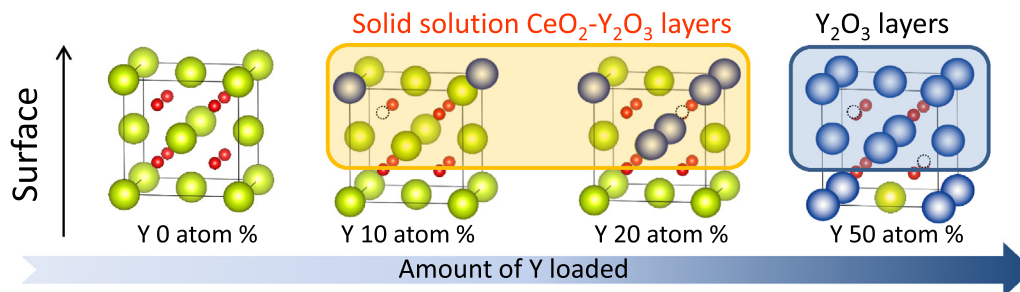
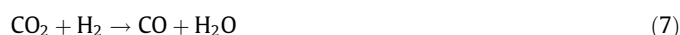
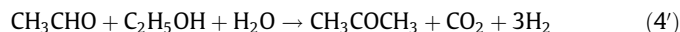


Fig. 6. Schematic surface structure of Y/CeO₂ catalysts prepared through the impregnation method. Surface oxygen ions are omitted for clarity.

degrees and the product yields would be attributed to the formation of undetected products such as carboxylic acids and esters. We indeed observed these products using an offline capillary GC system: However, the quantitative analyses were not conducted here because of too long intervals of the analyses.

The correlation of the product distribution with the contact time was examined using the continuous flow reactions to understand the reaction pathways yielding acetone, propene, and ethene. The results on the Y(20)/CeO₂ are shown in Fig. 7. The conversion levels of ethanol increased from 5% to 100% with increasing contact time, the selectivity of propene increased from 1% to 33%, and the selectivity of acetone decreased from 18% to 3%, indicating the possibility that acetone was an intermediate for propene formation. On the other hand, the selectivity toward ethene decreased from 60% to 40%. Small amounts of butenes (not shown) were formed in the experiments. No production of propene upon introduction of ethene onto the catalyst was also confirmed in a separated experiment. Both findings indicated little possibility of metathesis reaction of ethene and butenes to give propene.

The reaction pathways yielding acetone from ethanol have been suggested as Eqs. (3), (4), and (4') on oxide-based catalysts [2–6,9–12]. Propene can be formed from acetone through hydrogenation and subsequent dehydration, as described by Eq. (5) [9,10]. The comprehensive reaction for the propene formation is thus Eq. (6).



According to the reactions, the ratio of the total yield of propene and acetone (A_{C_3}) to those of CO₂ and CO (A_{CO_x}) should be 3:1, where contribution of the reverse water–gas shift reaction (Eq. (7)) was counted for the A_{CO_x} calculation. The calculated $A_{\text{C}_3/\text{CO}_x}$ values are listed in Table 1. The values on the catalysts active for the propene formation were 2.5–3.0. The good consistency indicated validity of the reaction pathways (3)–(7) and the estrangement from 3 would be due to the side reactions or the isobutene formation from acetone [10,11].

Three reaction sequences have been proposed for the formation of C_{2x-1} ketones from C_x-alcohols on oxide-based catalysts: (i) aldol reaction [5,6], (ii) Tishchenko reaction [2,3,44], and (iii) keto-nization reaction of carboxylic acids [45]. The possibility of the aldol reaction will be first discussed. The aldol reaction of acetaldehyde gives 3-hydroxybutylaldehyde, which can be converted to CH₃C(O)CH₂CHO or CH₃CH = CHCHO by dehydrogenation or dehydration. The latter does not give acetone, but the reaction of the former with water might yield acetone, CO₂, and H₂. Since unstable β-hydroxyaldehyde and β-ketoaldehyde could not be used as substrates, the products produced in Fig. 7 were carefully analyzed using the offline GC system. However, no production of these compounds was found, suggesting little possibility of the aldol reaction route. The formation of acetaldehyde, ethyl acetate, acetic acid, and 2-propanol was confirmed: Therefore, the possibilities of Tishchenko reaction route (via ethyl acetate) [2,3,44] and the keto-nization route (via acetic acid) [45] were investigated in the next section.

Pulse experiments were carried out on the Y(20)/CeO₂ using ethyl acetate (AcOEt), acetic acid (AcOH), and acetone as the substrates. AcOEt could be obtained from two acetaldehyde molecules through the Tishchenko reaction [2,3,44], as described by Eq. (8).



Fig. 8 shows the results for AcOEt as a function of contact time. In the absence of water, the major product was ethene irrespective of the contact time, although the yields considerably varied from 40% to 60%. The yield of acetone was high (~20%) at the short contact time of 0.11 s⁻¹, and the yields of propene were low (6–20%) compared to those in the flow reaction system. The co-feed of water with ethanol noticeably increased the yields of both propene and acetone to 10–20%. The results indicated the possibility that AcOEt was an intermediate for acetone and ethene formation.

The results of AcOH are also shown in Fig. 8. AcOH would hardly be generated from ethanol under the non-oxidative condition, but

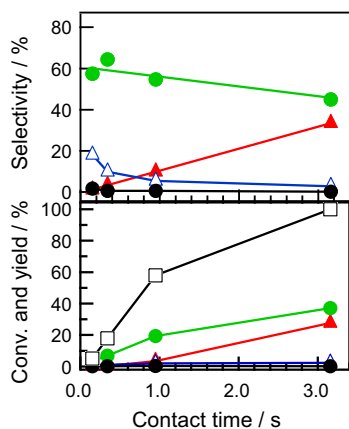


Fig. 7. Ethanol contact time dependence of the catalytic activity of Y(20)/CeO₂ for the continuous flow reactions. Reaction conditions: catalyst weight, 0.05–2.0 g; total flow rate, 12–32 ml min⁻¹; P_{EtOH}, 30 vol%; P_{H₂O}, 30 vol%; reaction temperature, 703 K. Symbols are the same as those in Fig. 1 except for ethanol (open black square).

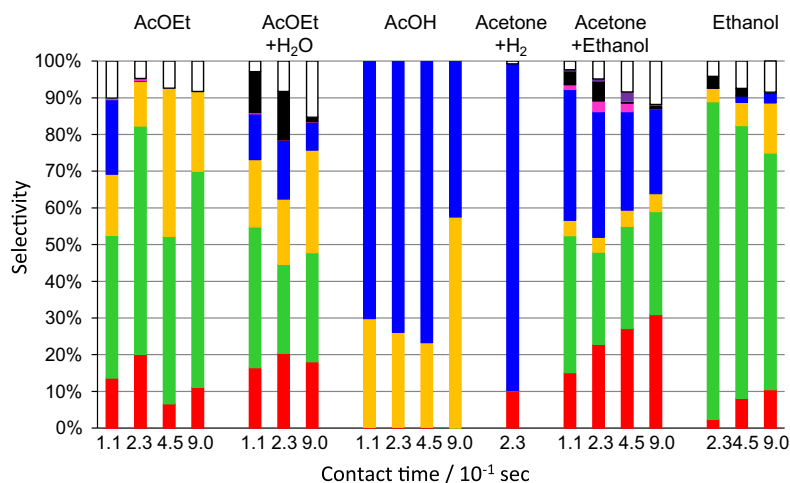
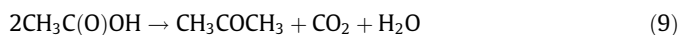
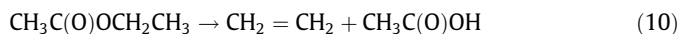


Fig. 8. Pulse experiment results for the Y(20)/CeO₂ as a function of contact time. Reactants are ethyl acetate (AcOEt), acetic acid (AcOH), acetone, and ethanol. As needed, water, H₂ gas, ethanol was fed with the reactants, such as AcOEt and acetone. Reaction conditions: pulse size, 2.0 μl, catalyst weight, 0.1 g; total flow rate, 10–80 ml min⁻¹; reaction temperature, 703 K. Red, propene; green, ethene; orange, CO₂; blue, acetone; pink, AcOH; black, ethanol; gray, AcOEt; purple, acetaldehyde; white, others. (For interpretation of the references to colour in this figure legend, the reader is referred to the web version of this article.)

in the presence of water, which is a by-product of ethanol dehydration, AcOH might be yielded through the direct reaction of an adsorbate CH₃CO with a surface OH group. All introduced AcOH was converted to acetone and CO₂ even at the short contact time, wherein the ratios of acetone produced to CO₂ were almost 3:1 (carbon basis) except for that at the long contact time. These results indicated the very easy and selective ketonization of AcOH (Eq. (9)), agreeing well with the results reported on ceria-based catalysts [45].



The following reaction pathways could be suggested on the basis of the above pulse experiments, although surface intermediates should be detected by for example IR measurements in the future. That is, AcOEt was converted to AcOH through elimination of ethene (Eq. (10)), and the subsequent self-ketonization of produced AcOH yielded acetone and CO₂ (Eq. (9)) [45].



Finally, the conversion of acetone to propene was confirmed to progress on the catalyst. Differently from the reported reaction [10], acetone gave only a small amount of propene in the presence of H₂ (propene yield was less than 10%), as shown in Fig. 8. In contrast, acetone could be converted to propene in the co-feed of ethanol, suggesting the reduction of acetone by ethanol and the subsequent dehydration of produced 2-propanol to propene. The former reaction is recognized as Meerwein–Ponndorf–Verley (MPV) reduction [46], and the possible reaction scheme is shown in Fig. 9. The active site could be the acid–base pair consisting of Ce³⁺ or Y³⁺ and O²⁻ ions, which was generated through the

formation of oxygen vacancy [47]. The adsorbed ethanol on the acid–base pair could reduce the acetone adsorbed on the acid site to 2-propanol, followed by the dehydration to give propene. The co-fed water might be involved in this reduction, but we have not understood yet the role of water at the molecular level.

Based on the above results and discussion, the following reaction pathways yielding propene from ethanol were suggested on the Y-modified ceria catalyst. Ethanol is dehydrogenated to acetaldehyde, and resulting acetaldehyde is dimerized to give ethyl acetate via a Tischenko reaction. Ethyl acetate is then decomposed to give ethene and acetic acid, the latter of which yields acetone and CO₂ through the ketonization reaction. Propene was produced by the MPV reduction of acetone by ethanol and the subsequent dehydration reaction. The present mechanism on Y/CeO₂ is different from that for Ni-MCM-41 [8] and Sc/In₂O₃ catalysts [9,10]. It should be noted that much amount of ethene was produced at the short contact time in the pulse reaction of ethanol (Fig. 8), which would suggest the presence of an alternative route (Eq. (10)) to form ethene through the simple dehydration of ethanol.

4. Conclusions

The addition effect of 31 metal ions on ceria catalysts was examined for the conversion of ethanol to propene. Twenty atom% Y-loaded ceria showed a good selectivity toward propene and remarkable durability in the absence of water. The maximum yield of propene on the Y(20)/CeO₂ was 37% at P_{EtOH} = P_{H₂O} = 30 vol%. The characterization revealed the formation of solid solution of CeO₂ and Y₂O₃. The elimination of strong acid sites originally existing on CeO₂ by the addition of Y₂O₃ would improve the

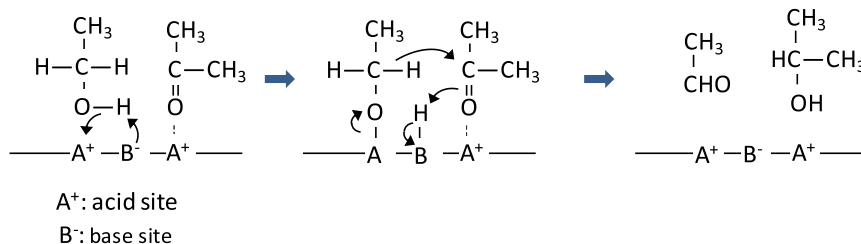


Fig. 9. Possible reaction mechanism for the Meerwein–Ponndorf–Verley reduction of acetone by ethanol.

durability of catalyst. The suggested reaction pathway was ethanol → acetaldehyde → ethyl acetate → acetic acid → acetone → 2-propanol → propene.

Acknowledgments

We greatly acknowledge Grants-in-Aid from the New Energy and Industrial Technology Development Organization (NEDO) and the Advanced Low Carbon Technology Program (JST) of Japan. The authors appreciate Dr. Tetsuo Suzuki and Mrs. Osamu Takahashi, Hiroshi Ohashi, and Takahiro Kakinuma of the NEDO research group for helpful discussions. The measurements of the XAFS spectra were performed under proposal numbers of 2009G661, and 2011G146 of the Photon Factory Program Advisory Committee.

Appendix A. Supplementary material

Supplementary data associated with this article can be found, in the online version, at <http://dx.doi.org/10.1016/j.jcat.2014.04.017>.

References

- [1] I. Chorkendorff, J.W. Niemantsverdriet, *Concepts of Modern Catalysis and Kinetics*, Wiley-VCH, Weinheim, Germany, 2007. pp. 1–21.
- [2] T. Nakajima, T. Yamaguchi, K. Tanabe, *J. Chem. Soc. Chem. Commun.* (1987) 394.
- [3] T. Nakajima, K. Tanabe, T. Yamaguchi, I. Matsuzaki, S. Mishima, *Appl. Catal.* 52 (1989) 237.
- [4] R. Sreerama-Murthy, P. Patnaik, P. Sidheswaran, M. Jayamani, *J. Catal.* 109 (1988) 298.
- [5] Y. Kamimura, S. Sato, R. Takahashi, T. Sodesawa, T. Akashi, *Appl. Catal. A* 252 (2003) 399.
- [6] Y. Kamimura, S. Sato, R. Takahashi, T. Sodesawa, M. Fukui, *Chem. Lett.* (2000) 232.
- [7] T. Tsuchida, J. Kubo, T. Yoshioka, S. Sakuma, T. Takeguchi, W. Ueda, *J. Catal.* 259 (2008) 183.
- [8] M. Iwamoto, K. Kasai, T. Haishi, *ChemSusChem* 4 (2011) 1055.
- [9] S. Mizuno, M. Kurosawa, M. Tanaka, M. Iwamoto, *Chem. Lett.* 41 (2012) 892.
- [10] M. Iwamoto, S. Mizuno, M. Tanaka, *Chem. Eur. J.* 19 (2013) 7214.
- [11] J. Sun, K. Zhu, F. Gao, C. Wang, J. Liu, C.H.F. Peden, Y. Wang, *J. Am. Chem. Soc.* 133 (2011) 11096.
- [12] F. Hayashi, M. Iwamoto, *ACS Catal.* 3 (2013) 14.
- [13] G.R.M. Dowson, M.F. Haddow, J. Lee, R.L. Wingad, D.F. Wass, *Angew. Chem. Int. Ed.* 52 (2013) 9005.
- [14] A.T. Aguayo, A.G. Gayubo, A. Atutxa, M. Olazar, J. Bilbao, *Ind. Eng. Chem. Res.* 41 (2002) 4216.
- [15] J. Bi, M. Liu, C. Song, X. Wang, X. Guo, *Appl. Catal. B* 68 (2011) 107.
- [16] M. Inaba, K. Murata, M. Saito, I. Takahara, *Green Chem.* 9 (2007) 638.
- [17] Z. Song, A. Takahashi, N. Mimura, T. Fujitani, *Catal. Lett.* 131 (2009) 364.
- [18] J.I. Di Cosimo, V.K. Diez, M. Xu, E. Iglesia, C.R. Apesteguia, *J. Catal.* 178 (1998) 499.
- [19] M.J.L. Gines, E. Iglesia, *J. Catal.* 176 (1998) 155.
- [20] A.S. Ndou, N. Plint, N.J. Coville, *Appl. Catal. A* 251 (2003) 337.
- [21] D.J. Elliott, F. Pennella, *J. Catal.* 119 (1989) 359.
- [22] Y. Wang, H. Kageyama, T. Mori, H. Yoshikawa, J. Drenman, *Solid State Ionics* 117 (2006) 1681.
- [23] R. Barthos, A. Széchenyi, F. Solymosi, *J. Phys. Chem. B* 110 (2006) 21816.
- [24] R.D. Shanon, *Acta Cryst.* A32 (1976) 751.
- [25] Z. Li, T. Mori, F. Ye, D. Ou, G.J. Auchterlonie, J. Zou, J. Drennan, *J. Phys. Chem. C* 116 (2012) 5435.
- [26] P. Li, I.-W. Chen, J.E. Penner-Hahn, *Phys. Rev. B* 48 (1993) 10074.
- [27] M. Malvestuto, R. Carboni, F. Boscherini, F. D'Acapito, S. Spiga, M. Fanciulli, A. Dimoulas, G. Vellianitis, G. Mavrou, *Phys. Rev. B* 71 (2005) 075318.
- [28] I. Kosacki, T. Suzuki, H.U. Anderson, H.P. Colombari, *Solid State Ionics* 149 (2002) 99.
- [29] Y. Naimai, K. Fukui, Y. Iwasawa, *J. Phys. Chem. B* 107 (2003) 11666.
- [30] A. Martinez-Arias, M. Fernandez-Garcia, L.N. Salamanca, R.X. Valenzuela, J.C. Conesa, J. Soria, *J. Phys. Chem. B* 104 (2000) 4038.
- [31] A.V. Soldatov, T.S. Ivachenko, S. Della Longa, A. Kotani, Y. Iwamoto, A. Bichcom, *Phys. Rev. B* 50 (1994) 5074.
- [32] The CN for cerium is calculated to be 7.4, assuming that 70% of Ce ions are Ce⁴⁺ (CN = 8.0) and the rest are reduced Ce³⁺ (CN = 6.0).
- [33] V. Perrichon, A. Laachir, G. Bergeret, R. Fréty, L. Tournayan, O. Touret, *J. Chem. Soc., Faraday Trans.* 90 (1994) 773.
- [34] R. Körner, M. Ricken, J. Nolting, I. Riess, *J. Solid State Chem.* 78 (1989) 136.
- [35] K. Sardar, H.Y. Playford, R.J. Darton, E.R. Barney, A.C. Hannon, D. Tompsett, J. Fisher, R.J. Kashtiban, J. Sloan, S. Ramos, G. Cibin, R.I. Walton, *Chem. Mater.* 22 (2010) 6191.
- [36] A. Pfau, K.D. Schierbaum, *Surf. Sci.* 321 (1994) 71.
- [37] M. Romeo, K. Bak, J. El Fallah, F. le Normand, L. Hilaire, *Surf. Interface Anal.* 20 (1993) 508.
- [38] M.I. Zaki, M.A. Hasan, F.A. Al-Sagheer, L. Pasupulety, *Colloids Surf. A* 190 (2001) 261.
- [39] C. Binet, M. Daturi, J.C. Lavalley, *Catal. Today* 50 (1999) 207.
- [40] C. Morterra, G. Cerrato, L. Ferroni, *J. Chem. Soc., Faraday Trans.* 91 (1995) 125.
- [41] H. Tsuneoka, K. Teramura, T. Shishido, T. Tanaka, *J. Phys. Chem. C* 114 (2010) 8892.
- [42] The requisite amount of Y₂O₃ (Y₂O_{3,surf}) for its monolayer coverage on the CeO₂ is calculated by the following equation on the assumption that Y³⁺ cations are isomorphously-substituted by Ce⁴⁺ cations on surface: Y₂O_{3,surf} (wt%) = 100 FW_{YO1.5} SD SA 10¹⁸/Av const. Here, FW_{YO1.5} is the formula weight of YO_{1.5}, 112.9, SD is the surface density of Y atom, 6.83 Y nm⁻², SA is the surface area of parent CeO₂, 85 m² g⁻¹, and Av const. is the Avogadro constant, 6.02 10²³. Details are shown in Ref. [43].
- [43] N. Naito, N. Katada, M. Niwa, *J. Phys. Chem. B* 103 (1999) 7206.
- [44] T. Seki, T. Nakajo, M. Onaka, *Chem. Lett.* 35 (2006) 824.
- [45] M. Renz, *Eur. J. Org. Chem.* (2005) 979.
- [46] D. Klomp, T. Mashmeyer, U. Hanefeld, J.A. Peters, *Chem. Eur. J.* 10 (2004) 2088.
- [47] S. Sato, F. Sato, H.i. Gotoh, Y. Yamada, *ACS Catal.* 3 (2013) 721.